EXPERIMENTAL STUDY OF STATISTICAL CHARACTERISTICS OF FILTERED RANDOM NOISE

NIC KNUDTZON

LOAN COPY

TECHNICAL REPORT NO. 115

JULY 15, 1949

RESEARCH LABORATORY OF ELECTRONICS
MASSACHUSETTS INSTITUTE OF TECHNOLOGY

MASSACHUSETTS INSTITUTE OF TECHNOLOGY

Research Laboratory of Electronics

Technical Report No. 115   July 15, 1949

EXPERIMENTAL STUDY OF STATISTICAL CHARACTERISTICS
OF FILTERED RANDOM NOISE

Nic Knudtzon

Abstract

Envelope distributions, zero-crossings, autocorrelation and power spectra have been obtained experimentally for filtered random noise from a gas tube, amplifier, resistor, space-charge limited and temperature limited diode, and Si-crystal. Two types of filters have been used: low-pass filters with cut-off frequencies in the range 10-100 kc, and single-tuned circuits with center frequency 20.4 kc and Q ranging in steps from 9.9 to 108. Single-sweep photographs of typical waveforms both of narrow-band and broadband noise are included. The envelope distributions have been measured by sampling the envelope electronically with the instantaneous noise voltage, and the average zero-crossing frequency by counting the number of peaks exceeding zero level. Autocorrelation functions have been recorded by an electronic correlator, and transformed to power spectra by means of an electronic differential analyzer. The results are in agreement with the existing macroscopic theory for random noise in linear systems.

TABLE OF CONTENTS

EXPERIMENTAL STUDY OF STATISTICAL CHARACTERISTICS
OF FILTERED RANDOM NOISE

INTRODUCTION

Fluctuation noise represents the inherent limiting factor in systems for the transmission of information. This fact has been realized for some time, and is particularly emphasized in the statistical theory of communication originated by Wiener and Shannon.

Practical application of this new theory requires the knowledge of statistical data for different types of messages and noise. Because of this, and as a part of the research program of the R.L.E. Communications Group, an experimental study of filtered random noise in linear systems has been carried out.

The phenomenon of spontaneous irregular fluctuations was first observed in mechanical systems as Brownian motion (1827), which after much mysterious speculation was explained qualitatively by Delsaux fifty years later and quantitatively by Smoluchowski and Einstein (1905-1906). The latter also predicted the existence of corresponding electrical phenomena, which actually were observed as soon as measuring devices of sufficient sensitivity became available. Schottky (1918) and Nyquist (1928) derived expressions for the rms value of shot and thermal noise respectively, and Moullin reports in his book (1938) some experiments, mostly of academic character, undertaken in connection with these formulas. With the recognition of the practical importance of random noise considerable effort was directed toward developing a complete theory of its statistical characteristics and its influence on other stationary time series. Very little is reported, however, on corresponding measurements with a desired degree of accuracy.

Present day experimental techniques make it possible to eliminate the abnormally large discrepancy between the status of theoretical knowledge and that of experimental knowledge of random noise. As a preliminary step in this direction, envelope distribution, average zero-crossing frequency, autocorrelation and power spectra were measured and photographs taken of fluctuation noise from a gas tube, amplifier, resistor, space-charge limited and temperature limited diode and Si-crystal after different low-pass and band-pass filters.

It is hoped that experiments will be continued and extended to nonlinear systems. Therefore some details of the difficulties encountered, which are likely to occur in statistical measurements, and their possible remedies are discussed.

The report is divided into three parts. Part 1 contains a summary of pertinent theoretical results, a description of the different noise sources, filters and amplifiers, and single-sweep photographs. Part 2 describes the noise distribution analyzer and the curves obtained for the envelope distributions. Part 3 is concerned with the statistical characteristics which are dependent on the system damping: zero-crossing frequency counted by the noise distribution analyzer, autocorrelation functions recorded by an electronic correlator and transformed to power spectra by an electronic differential analyzer.

PART 1. THEORY, NOISE SOURCES AND FILTERS, PHOTOGRAPHS

1.1 Review of Pertinent Theoretical Results

A distinction will be made between narrow-band and broadband noise. In the first case the bandwidth W between the half-power points is much less than the center or resonance frequency $f_o = \omega_o/2\pi$ of the filter through which the noise is passed; in the latter W is greater than or equal to f_o.

1.11 Representation of noise voltage

A Fourier series analysis is made of successive sections of length T of an infinitely long record of random noise.

For the first section it is found

$$v_1(t) = \sum_{n=1}^{N} (a_{1n} + j\, b_{1n})\, \epsilon^{j\omega_n t}$$

where the a_{1n}'s and b_{1n}'s have certain fixed values and $\omega_n = 2\pi f_n = 2\pi \frac{n}{T}$.

For the second section coefficients a_{2n} and b_{2n} are obtained, and so on.

The fundamental assumptions for existing mathematical analysis of random noise can be expressed by the mutual independence of the coefficients a_n and b_n for different sections, this statistical distribution being normal around zero with standard deviation equal to $\sqrt{\Phi(f_n)\, 1/T}$, where $\Phi(f_n)$ is the power spectrum of the noise. This hypothesis leads to the two known representations of the instantaneous noise voltage

$$v(t) = \sum_{n=1}^{N} (a_n + j\, b_n)\, \epsilon^{j\omega_n t} \tag{1-1a}$$

$$= \sum_{n=1}^{N} c_n \cos(\omega_n t - \phi_n) \tag{1-1b}$$

where $c_n = \sqrt{2\Phi(f_n)\frac{1}{T}}$ and ϕ_n is a random phase angle, uniformly distributed over the range $(0, 2\pi)$.

For narrow-band noise these expressions may be conveniently transformed in the following way

$$v(t) = \sum_{n=1}^{N} (a_n + j\, b_n)\, \epsilon^{j(\omega_n - \omega_o)t}\, \epsilon^{j\omega_o t}$$

$$= \sum_{n=1}^{N} \left[a_n\, \epsilon^{j(\omega_n - \omega_o)t} + j\, b_n\, \epsilon^{j(\omega_n - \omega_o)t} \right] \epsilon^{j\omega_o t}$$

$$= \sum_{n=1}^{N} \left[a_n(t) + j\, b_n(t) \right] \epsilon^{j\omega_o t} \tag{1-2}$$

where $a_n(t)$ and $b_n(t)$ are orthogonal functions of time. The envelope of $v(t)$ is then

$$V(t) = \sqrt{\left[\sum_{n=1}^{N} a_n(t)\right]^2 + \left[\sum_{n=1}^{N} b_n(t)\right]^2}$$

$$= \sqrt{\left[a(t)\right]^2 + \left[b(t)\right]^2} \quad . \tag{1-3}$$

Thus, the narrow-band noise has the character of an amplitude- and frequency-modulated wave with envelope $V(t)$. For an ideal rectangular band-pass filter the average "period" of the envelope is a linear function of the bandwidth only. Although mathematically valid Eqs. (1-2) and (1-3) have no physical meaning for broadband noise since the period of the instantaneous noise voltage is of the same order of magnitude as the period of the envelope.

1.12 Amplitude distributions

The distribution function $P_\xi(X)$ of the variable $\xi(t)$ is defined as

$$P_\xi(X) = \text{probability}\left[\xi \leq X\right] = 1 - \text{probability}\left[\xi \geq X\right]$$

and is equal to the fraction of time $\xi(t)$ is less than the level X.

Furthermore, $dP_\xi(X) = p_\xi(X)\,dX = \text{probability}\left[X < \xi < X + dX\right]$ where $p_\xi(X) = P'_\xi(X)$ is called the distribution density.

On the basis of the fundamental assumption for mathematical analysis of random noise and the Gaussian addition theorem it can be easily shown that the distribution density for the instantaneous noise voltage is a Gaussian curve.

$$p_v(X) = \frac{1}{\mathcal{U}\sqrt{2\pi}} \exp\left(-\frac{X^2}{2\mathcal{U}^2}\right) \tag{1-4a}$$

where

$$\mathcal{U} = \sum_{n=1}^{N} \Phi(f_n) \frac{1}{T}$$

is the rms value of the noise or normalized with respect to $\mathcal{U}$

$$p_v(x) = \frac{1}{\sqrt{2\pi}} \exp\left(-\frac{x^2}{2}\right) \tag{1-4b}$$

where $x = X/\mathcal{U}$.

The distribution density for the noise envelope can be derived from Eq. (1-3) and (1-4a) as follows: the probability that the point $[a(t), b(t)]$ lies in the elementary rectangle $dX_a\,dX_b$ is

$$\frac{dX_a\,dX_b}{2\pi\mathcal{U}^2} \exp\left(-\frac{X_a^2 + X_b^2}{2\mathcal{U}^2}\right)$$

-3-

or by introducing polar coordinates

$$X_a = X \cos \theta$$

$$X_b = X \sin \theta$$

the probability that V(t) lies in the angular sector $dX d\theta$ is

$$\frac{d\theta}{2\pi} \frac{X dX}{\mathcal{U}^2} \exp\left(-\frac{X^2}{2\mathcal{U}^2}\right)$$

X and θ are independent variables, θ being uniformly distributed over the range $(0, 2\pi)$. Therefore the distribution density for the envelope is

$$p_V(X) = \frac{X}{\mathcal{U}^2} \exp\left(-\frac{X^2}{2\mathcal{U}^2}\right) \int_0^{2\pi} \frac{d\theta}{2\pi}$$

$$= \frac{X}{\mathcal{U}^2} \exp\left(-\frac{X^2}{2\mathcal{U}^2}\right) \tag{1-5a}$$

or normalized with respect to $\mathcal{U}$

$$p_V(x) = x \exp\left(-\frac{x^2}{2}\right) \ . \tag{1-5b}$$

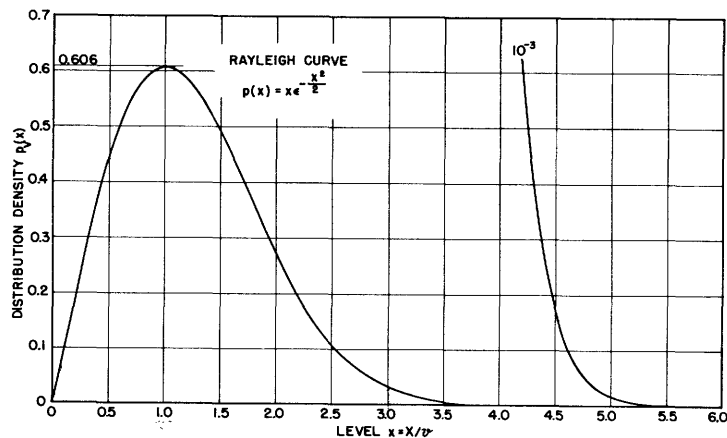This is a Rayleigh curve as plotted in Fig. 1-1.

Fig. 1-1 Normalized envelope distribution density, Rayleigh curve
$$p(x) = x\epsilon - x^2/2.$$

The most probable level for the envelope is equal to the rms value of the noise. Theoretically there is a finite probability for noise peaks of any finite height, but zero probability for zero level.

The distribution function for the envelope is

$$P_V(X) = 1 - \int_X^\infty dp_V(X) = 1 - \exp\left(-\frac{X^2}{2\sigma^2}\right) \qquad (1\text{-}6a)$$

or normalized

$$P_V(x) = 1 - \exp\left(-\frac{x^2}{2}\right) \quad . \qquad (1\text{-}6b)$$

1.13 Average zero-crossing frequency

The average zero-crossing frequency f_z is equal to the number of peaks of the instantaneous noise voltage exceeding zero level per second.

Rice (1) (Sec. 3.4) has determined the expected number of zero-crossings per second to be

$$2\left[\frac{\int_0^\infty f^2 \, \Phi(f) \, df}{\int_0^\infty \Phi(f) \, df}\right]^{1/2} \quad . \qquad (1\text{-}7)$$

It is interesting to observe that the average zero-crossing frequency is equal to the "gyration frequency" (i.e. the frequency coordinate of the center of percussion) of the associated power spectrum.

1.14 Autocorrelation function and power spectrum

The autocorrelation function $\phi(\tau)$ of a time function $v(t)$ is defined as the time average of the product of all pairs of points of $v(t)$ separated by an interval τ

$$\phi(\tau) = \lim_{T \to \infty} \frac{1}{2T} \int_{-T}^{T} v(t) \, v(t + \tau) \, dt \quad . \qquad (1\text{-}8a)$$

It may also be expressed by the conditional probability $P_2(X_1, X_2; \tau)$ as follows

$$\phi(\tau) = \iint_{-\infty}^{\infty} X_1 \, X_2 \, P_2 \, (X_1, X_2; \tau) \, dX_1 \, dX_2 \quad . \qquad (1\text{-}8b)$$

The power spectrum $\Phi(f)$ is defined as the amount of power per unit bandwidth as a function of frequency.

The Wiener-Khintchine theorem establishes the Fourier transform relationship between these two functions

$$\phi(\tau) = \int_{-\infty}^{\infty} \Phi(\omega) \exp(j\omega\tau) \, d\omega \qquad (1\text{-}9)$$

$$\Phi(\omega) = \frac{1}{2\pi} \int_{-\infty}^{\infty} \phi(\tau) \exp(-j\omega\tau) \, d\tau \quad . \qquad (1\text{-}10)$$

Consider the simple case of narrow-band noise after a rectangular filter of width W and center frequency $f_o = \omega_o/2\pi$. The output power spectrum is

$$\Phi_o(\omega) = \begin{cases} 0 & \omega_o + \pi W < \omega \\ \Phi_i(\omega) & \omega_o - \pi W < \omega < \omega_o + \pi W \\ 0 & \omega < \omega_o - \pi W \end{cases} .$$

For an input power spectrum $\Phi_i(\omega) = a = \text{constant}$, the autocorrelation function is

$$\phi(\tau) = a \int_{\omega_o - \pi W}^{\omega_o + \pi W} \cos \omega\tau \, d\omega = a \left[\frac{\sin \omega\tau}{\tau} \right]_{\omega_o - \pi W}^{\omega_o + \pi W}$$

$$= 2a \frac{\sin \pi W\tau}{\tau} \cos \omega_o t$$

$$= 2a\pi W \left(\frac{\sin \pi W\tau}{\pi W\tau} \right) \cos \omega_o t$$

which is a cosine wave of frequency ω_o modulated by $\dfrac{\sin \pi W\tau}{\pi W\tau}$.

The autocorrelation function for narrow-band noise through a single-tuned circuit with $Q = R/\omega_o L$ can be derived in the same way. The output power spectrum is

$$\Phi_o(\omega) = \frac{L^2 \omega^2}{\left(1 - \dfrac{\omega^2}{\omega_o^2}\right)^2 + \left(\dfrac{\omega^2}{Q\omega_o}\right)^2} \, \Phi_i(\omega) .$$

For an input power spectrum $\Phi_i(\omega) = a = \text{constant}$ the autocorrelation function is a damped cosine wave (2).

$$\phi(\tau) = \frac{\pi a L^2 \omega^3 Q}{2} \exp\left(- \frac{\omega_o \tau}{2Q}\right) \cos\left(\omega_o \tau - \frac{1}{2Q} \sin \omega_o \tau\right)$$

$$\approx \frac{\pi a L^2 \omega^3 Q}{2} \sqrt{1 + \left(\frac{1}{2Q}\right)^2} \exp\left(- \frac{\omega_o \tau}{2Q}\right) \cos\left(\omega_o \tau - \frac{1}{2Q}\right) . \qquad (1\text{-}12)$$

For broadband noise with rms value $\mathcal{V}$ and rectangular power spectrum of width W, the power spectrum and autocorrelation function are

$$\Phi(\omega) = \begin{cases} \mathcal{V}/2\pi W & 0 < \omega < 2\pi W \\ 0 & 2\pi W < \omega \end{cases}$$

$$\phi(\tau) = \frac{\mathcal{V}}{2\pi W} \int_0^{2\pi W} \cos \omega\tau \, d\omega = \frac{\mathcal{V}}{2\pi W} \left[\frac{\sin \omega\tau}{\tau} \right]_0^{2\pi W}$$

$$= \mathcal{V} \frac{\sin 2\pi W\tau}{2\pi W\tau} . \qquad (1\text{-}13)$$

In the extreme broadband case (purely random noise) there is no correlation, and $\phi(\tau)$ is a delta-function at $\tau = 0$. This case is only a mathematical abstraction however, as all noise sources are limited in frequency.

These examples clearly demonstrate that the autocorrelation function is an important statistical parameter with distinct features expressing the characteristics of the output time function.

Furthermore, the autocorrelation function has proved itself to be a valuable tool in theoretical investigations. Equations (1-8) and (1-10) constitute the key equations for the so-called "correlation method": the power spectrum $\Phi(f)$ can be determined via $\phi(\tau)$ which in many cases has been found quite easily by statistical considerations.

1.2 Noise Sources and Preamplifiers

Table 1-1 shows diagrams for the six noise sources investigated and their associated preamplifiers. Although the aim is to investigate noise rather than the physics of noise sources, some remarks on these are included.

1.21 Gas tube 884

The 884 is a thyratron originally built for control purposes. Due to the high noise level it has also been used as a noise source especially for jamming.

The mechanism of its noise generation is not thoroughly understood. Cobine and Gallagher (3)(4) have found spectra of the general character shown in Fig. 1-2, where

Fig. 1-2 Typical noise spectrum for gas tube 884.

the mode at A (somewhat below 400 kc) is due to plasma oscillations, and at B (around 700 kc) to cathode oscillations. The former can be suppressed by a magnetic field of proper strength and direction. The preferable plate current is reported to be in the range 25-40 ma.
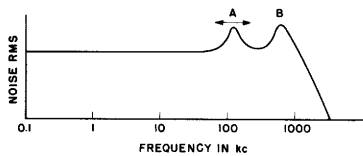
The author has found the gas tube 884 to be highly individual with respect to noise output, location and stability of the arc. Out of ten tubes, the best was selected and used throughout the project.

The filament was heated by d-c, which had to be carefully adjusted. Fig. 1-3 shows

Fig. 1-3 Filament control.

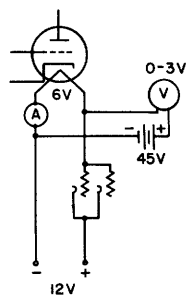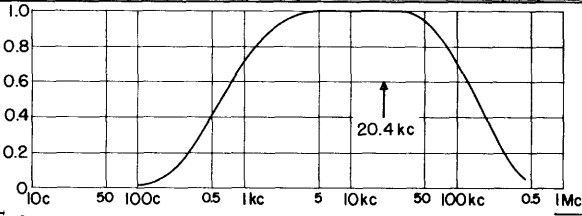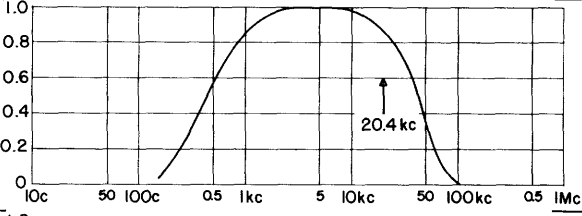verniers and arrangement used to improve accuracy of readings of applied voltage. The plate current was held at 30 ma.
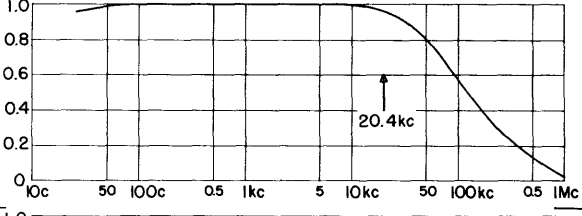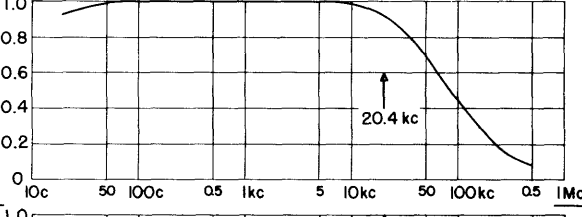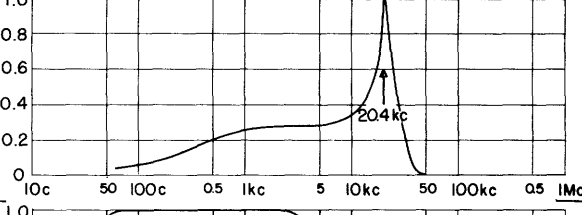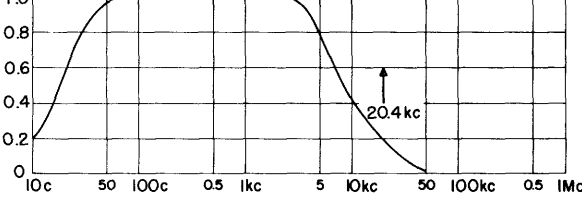
In spite of many precautions, the 884 tube gave rise to considerable trouble due to its unstable nature and oscillations. This is pointed out in Part 3 in connection with the results for average zero-crossing frequency and power spectra. Although the gas tube 884 finally was controlled, it may be concluded that

TABLE I-I: NOISE SOURCES	
TYPE	DIAGRAM
GAS TUBE 884	+200V, 2K, Ⓐ30mA, 5K, Ⓥ, 884, 0.6A
BALLANTINE AMPLIFIERS MODEL 300 SHOT AND THERMAL NOISE	INPUT SHORTED
G.R. AMPLIFIER TYPE 1231-B THERMAL NOISE	G.R. AMPLIFIER INPUT OPEN SHIELDED BALLANTINE DECADE AMPLIFIER MOD. 220 — BALLANTINE AMPLIFIER MOD. 300 PRE-AMPLIFIER
EIMAC 15E a) SPACE CHARGE ⎫ LIMITED b) TEMPERATURE ⎭ SHOT NOISE	+200V, 1K, 15K, Ⓐ, 5K, Ⓥ, 15E, TRANSFORMER BALLANTINE DECADE AMPLIFIER MOD. 220 — BALLANTINE AMPLIFIER MOD. 300 PRE-AMPLIFIER
SI-CRYSTAL	+1.5V D.C., 10K, SI, 220, 10K, 13μμf BALLANTINE DECADE AMPLIFIER MOD. 220 — BALLANTINE AMPLIFIER MOD. 300 PRE-AMPLIFIER

TABLE I-2: TRANSFER CHARACTERISTICS

EQUIPMENT	NORMALIZED CURVES	CODE NUMBER
AMPLIFIER WITHOUT BUTTERWORTH BAND-PASS FILTER (FIG. I-8)		I
AMPLIFIER WITH BUTTERWORTH BAND-PASS FILTER (FIG. I-8)		2
BALLANTINE AMPLIFIER MODEL 300 (TABLE I-1)		3
BALLANTINE DECADE AMPLIFIER MODEL 220 (TABLE I-1)		-4
TRANSFORMER x BALLANTINE DECADE AMPL. x BALLANTINE AMPLIFIER (TABLE I-1)		5
G.R. AMPLIFIER TYPE 1231-B (TABLE I-1)		6

PREAMPLIFIERS (rows 3–5)

NOISE SOURCE (row 6)

it was an unhappy choice for long-time statistical measurements. Later work in this Laboratory has shown that gas tube 6D4 in a magnetic field probably is superior.

1.22 Ballantine amplifiers in cascade

With the input terminals shorted and grounded, the output is mainly amplified shot noise from the first tube. After a couple of hours of operation to reach temperature equilibrium, this arrangement proved to be a stable, powerful and conveniently regulative source for random noise.

The frequency characteristic is shown in Table 1-2.

1.23 G. R. amplifier, type 1231-B

The voltage ratio between output noise with input terminals open and shorted was 5, indicating that in the first case the output substantially consisted of amplified thermal noise from the input grid resistor.

The amplifier was battery-operated, the frequency characteristic is shown in Table 1-2. Acoustic padding was used to avoid microphonics of the same order of magnitude as the noise.

1.24 Eimac 15E

This tube was selected for generation of space-charge and temperature limited noise for the following two reasons: (a) it has high plate dissipation allowing for high plate current, and (b) it has pure tungsten filament. (The presence of an oxide coating may lower the work function locally and cause undesired and uncontrollable modulation of the emission current.)

The noise rms value over a bandwidth W = 100 kc is

$$\mathcal{V} = R_D \sqrt{2eIW} \times \Gamma$$

$$= R_D \sqrt{I} \times 0.568 \; 10^{-8} \times \Gamma \quad \text{volts} \tag{1-14}$$

where

$R_D \Omega$ = plate resistance of diode

I ma = plate current

Γ = space-charge reduction factor.

It will be seen from the sketch in Fig. 1-4 that in space-charge limited operation the current I is critically affected by the plate voltage and is essentially independent of minor changes in the filament voltage, whereas under temperature limited conditions just the opposite is true. It is therefore easy to check that the tube is working in the desired region.

Part of the measured characteristic in the space-charge limited region is plotted in Fig. 1-5. It is found that I = 45 ma makes $R_D \sqrt{I}$ and hence the noise output a maximum.
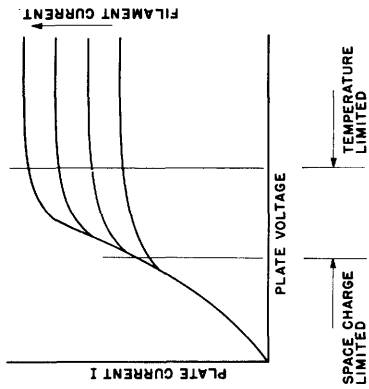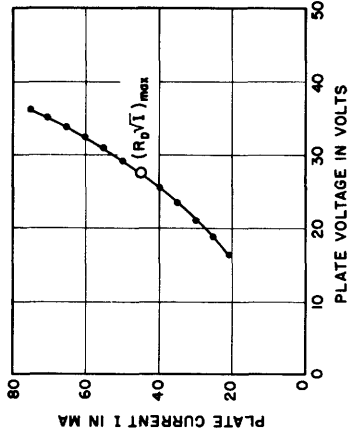
Fig. 1-5 Measured characteristic in space-charge limited region for Eimac 15E.

$(R_D\sqrt{I})_{max}$

PLATE VOLTAGE IN VOLTS

PLATE CURRENT I IN MA
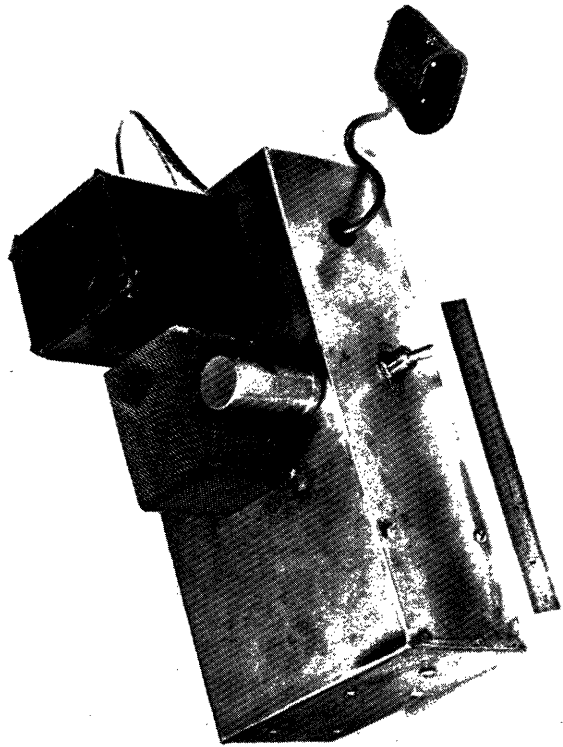
Fig. 1-7 Si-crystal noise source.

FILAMENT CURRENT

TEMPERATURE LIMITED

PLATE VOLTAGE

SPACE CHARGE LIMITED

PLATE CURRENT I

Fig. 1-4 Typical characteristics for diode.

Fig. 1-6 Eimac 15E noise source.

-11-

Fig. 1-8 Circuit diagram for filters and amplifier.

FILAMENTS OPERATED ON D-C

SINGLE-TUNED CIRCUIT F_1

W_c	Q	R_x kΩ	R_y kΩ
188	108	2700	—
433	47	1600	2700
630	32	1300	1000
766	26.6	1200	750
1030	19.8	1000	560
1250	16.3	910	430
1480	13.8	820	360
1740	11.7	820	300
1920	10.6	750	270
2070	9.9	750	240

W = BANDWIDTH MEASURED BE-
TWEEN HALF-POWER POINTS $= f_o/Q$

FROM NOISE SOURCE

WITH BUTTERWORTH LOW-PASS FILTER

WITHOUT BUTTERWORTH LOW-PASS FILTER

+200V

TO SLICER CORRELATOR

TO OSCILLOSCOPE

THERMOCOUPLE

+400V

-150V

6AG7

807

6SJ7

6SJ7

F_1

F_2

-12-

In the space-charge limited case the noise voltage at the output of the transformer (see diagram in Table 1-1) was 7 times greater than the noise level of the Ballantine decade amplifier. In the temperature limited case the ratio was even higher.

The transfer characteristic of the transformer and the cascaded preamplifiers is given in Table 1-2. The peak is due to resonance in the transformer.

Figure 1-6 shows a picture of the Eimac 15E noise source with the tube located inside the wire mesh screen. By means of a control system similar to that in Fig. 1-3 the filament and plate current were held at 3.80 amp and 35 ma respectively for space-charge limited operation and at 2.27 amp and 6.12 ma for temperature limited operation.

1.25 Si-crystal

Figure 1-7 is a photograph of this source, which originally was designed for rough measurements of noise figures. It was found to be highly unstable with the rms noise voltage varying abruptly and uncontrollably $\pm$ 15 percent after intervals ranging from several seconds to around 10 minutes. A direct current of 50 μa was forced through the crystal in the reversed direction.

1.3 Investigated Frequency Region

Noise from gas tube 884 is supposed to have an almost flat power spectrum up to around 100 kc, although plasma oscillations may occur at somewhat lower frequencies. Thermal and shot noise should theoretically be independent of the location of the passband. Crystal noise is mainly concentrated in the lower part of the spectrum.

Inasmuch as it is convenient to use the same measuring equipment for all six noise sources, it was decided to work in the region around 20 kc, which in addition has certain technical advantages, among which is the avoidance of microphonics and ripple.

1.4 Filters and Amplifier

The noise from the sources is, if necessary, passed through the preamplifiers as indicated in Table 1-1 before entering the band-pass filter. Figure 1-8 shows this filter and the successive stages of amplification.

1.41 Filters

Band-pass filter F_1 is a single-tuned circuit centered at 20.4 kc. By shunting its toroid coil with fixed resistors, the Q can be varied in 10 discrete steps between 108 and 9.9 as tabulated in Fig. 1-8.

In spite of the considerable attenuation of high frequency components by the single-tuned circuit, these caused disturbances especially in the case of gas tube noise. For this reason the Butterworth low-pass filter was inserted at F_2. Results obtained both with and without the Butterworth filter will be presented in later parts.

1.42 Amplifier

The amplifier was designed to obtain a large linear dynamic range in order to accommodate the highest peaks of interest.

Circuit details are given in Fig. 1-8, and the transfer characteristics with and without the Butterworth low-pass filter are plotted in Table 1-2.

1.5 Transfer Characteristics

All pertinent transfer characteristics (voltage ratio as a function of frequency) are assembled in Table 1-2, and given a code number indicated in the last column. For simplicity reference will be made to these numbers, and Q of the particular single-tuned circuit, if inserted, indicated after a comma. For example: filter No. 1, 9.9 refers to transfer characteristic for amplifier without Butterworth low-pass filter, single-tuned circuit with Q = 9.9; filter No. 5 × 2 refers to transfer characteristic for transformer, Ballantine decade amplifier, Ballantine amplifier and amplifier with Butterworth filter in cascade, no single-tuned circuit.

1.6 Photographs of Noise

The display of filtered noise on an oscilloscope with continuous sweep is usually referred to as "grass" because of its disorderly and apparent non-periodic appearance.

It was pointed out in Sections 1.11 and 1.14 that noise is always autocorrelated. In particular narrow-band noise has the character of an amplitude- and frequency-modulated wave. In order to get some conception of this nature, a series of single-sweep photographs has been taken both for narrow-band and broadband noise from the different sources as displayed on an Allen DuMont oscilloscope, Type 279.

The rms value of the filtered noise was in all cases 2.7 volts. Two fixed sweep speeds, here referred to as "slow" and "fast", were used, the former emphasizing details of the envelope and the latter of the instantaneous voltage. For each particular noise source and filter combination, many single-sweep exposures were made, and the most typical one was chosen.

In Table 1-3 the photographs for all sources, except gas tube 884, are placed together for comparison. In the narrow-band cases there appear to be no pronounced distinctive features. Furthermore, it is noticed that the general character coincides well with the interpretations noted for Eqs. (1-2) and (1-3), with the exception of some very slight perturbations on the otherwise smooth waveforms for the lowest Q's. For broadband noise there is considerable variation in appearance. These differences are to be expected and can be explained in terms of the associated transfer characteristics shown in Table 1-2.

The displays of the different types of narrow-band noise just considered are essentially unaltered for transfer characteristic No. 1 instead of No. 2, i.e. with the Butterworth low-pass filter left out. For noise from gas tube 884, however, there is a definite difference as readily seen from Table 1-4. The irregularities in the waveforms to the left indicate the presence of high frequency components, which are not sufficiently attenuated by the single-tuned circuit alone.
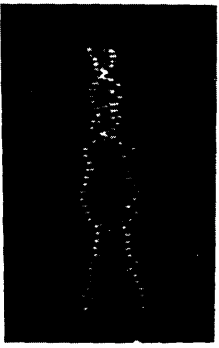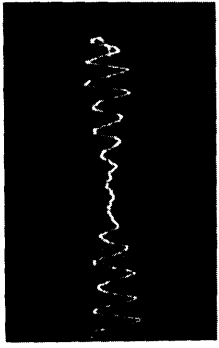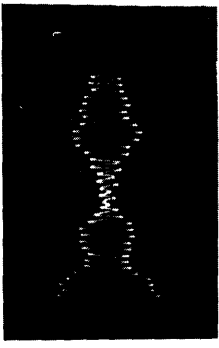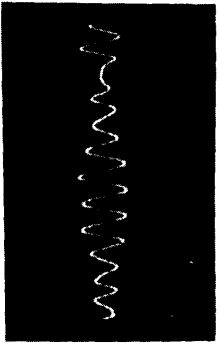
FILTERS : SEE CODE NUMBER FOR EACH PICTURE
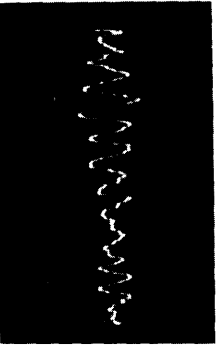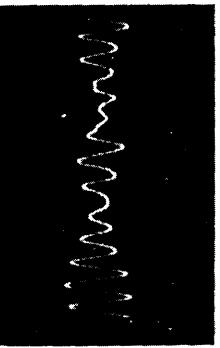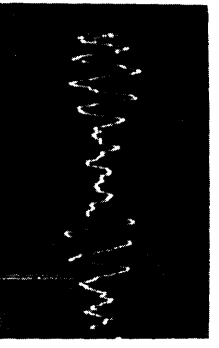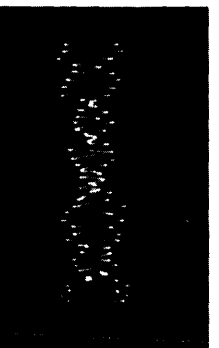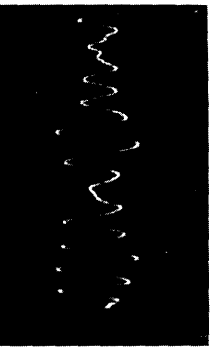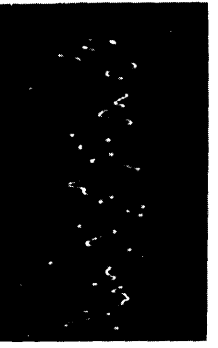
TABLE I-3 : SINGLE-SWEEP PHOTOGRAPHS OF NOISE FROM DIFFERENT SOURCES

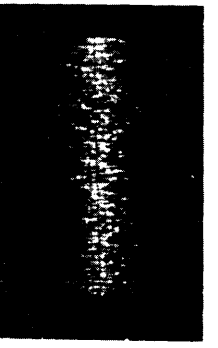| SHOT AND THERMAL NOISE FROM BALLANTINE AMPLIFIERS		THERMAL NOISE FROM G.R. AMPLIFIER 1231-B		SPACE CHARGE LIMITED SHOT NOISE FROM EIMAC 15E		TEMPERATURE LIMITED SHOT NOISE FROM EIMAC 15E		CRYSTAL NOISE FROM S1-CRYSTAL	
SLOW	FAST	SLOW	FAST	SLOW	FAST	SLOW	FAST	SLOW	FAST
2,108		4×3×2,108		5×2,108		5×2,108		4×3×2,108	
2,26.6		4×3×2,26.6		5×2,26.6		5×2,26.6		4×3×2,26.6	
2,9.9		4×3×2,9.9		5×2,9.9		5×2,9.9		4×3×2,9.9	
2,—		4×3×2,—		5×2,—		5×2,—		4×3×2,—	
1,—		4×3×1,—		5×1,—		5×1,—		4×3×1,—	

TABLE I-4: SINGLE SWEEP PHOTOGRAPHS OF NOISE FROM GAS TUBE 884

R.M.S. = 2.7 VOLTS

$Q_{VAR.}$	FILTER : I, $Q_{VAR.}$		FILTER : 2, $Q_{VAR.}$	
	SLOW	FAST	SLOW	FAST
108				
26.6				
9.9				
—				

PART 2. ENVELOPE DISTRIBUTION

2.1 Previous Experiments

Some early investigators have reported an apparent maximum of noise peaks at
4 - 4.5 times the rms value and introduced the corresponding so-called noise "crest
factor". However, as pointed out in connection with Eq. (1-5) there is no theoretical
justification for this concept. Therefore, either the theory is in error, or the measure-
ments so far have not been of sufficient sensitivity and duration. This is a question of
practical interest as well as academic.

During the fall of 1947 efforts were made to study the amplitude distributions in this
Laboratory (5)(6). T. P. Cheatham, Jr. took moving pictures of the display of random
noise on an oscilloscope and counted the number of intersections at different levels on
an enlarged copy. Due to the tedious amount of work the total number of samples was
limited to about 500 at relatively low levels, leading to results (among others) for the
envelope distribution density as shown in Fig. 2-1. No conclusions could be drawn from
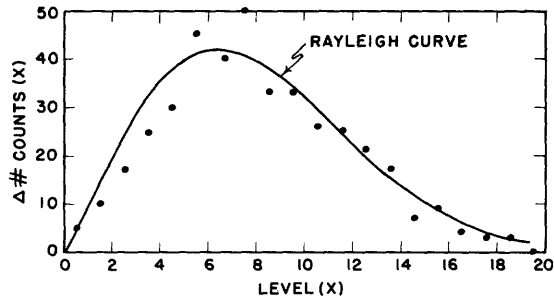

Fig. 2-1

**Typical points for the noise envelope
distribution density obtained by
photograph-counting technique.**

this and similar plots with respect to the abso-
lute or systematic nature of the discrepancy
between the counted points and the theoretical
curve. D. F. Winter scanned an oscilloscope
display of the time function with a phototube
measuring device. This method was not directed
toward great accuracy, but did afford speed
and flexibility. In both these experiments it
was assumed that the display on the scope is
an accurate reproduction of the applied noise
voltage.

Later the author has become aware of the
works of Pumper (7) and Fürth and MacDonald
(8), who have attacked the problem in very similar ways and arrived at results with the
same degree of uncertainty to those just described. To the author's knowledge these
are the only published papers on experimental studies of the statistics of noise.

It was soon realized that any improvement in techniques required a combination of
both speed and accuracy. A natural way* to get a sufficient number of samples is to
perform the slicing and counting electronically at the same rate as that at which the
noise peaks actually occur. The noise distribution analyzer which is described below is
a machine of this type for experimental determination of the noise envelope distribution.

---

* Originally suggested by T. P. Cheatham, Jr. and K. Boyer, from whose preliminary
  measurements parts of this research grew. They used modified apparatus available
  in the laboratory, and concluded that special and more adequate equipment was
  necessary.

2.2 Basis for Experimental Technique

Narrow-band noise has according to Eq. (1-2) and the photographs in Section 1.6 the character of a smooth wave, the envelope of which is V(t). The method which suggests itself for measuring the envelope distribution is therefore to sample the envelope electronically with the instantaneous noise voltage.

Figure 2-2 shows the block diagram, with associated waveforms for the noise distribution analyzer, built after this principle. The filtered and amplified random noise is fed into the slicer which only passes peaks higher than the level X set by the level
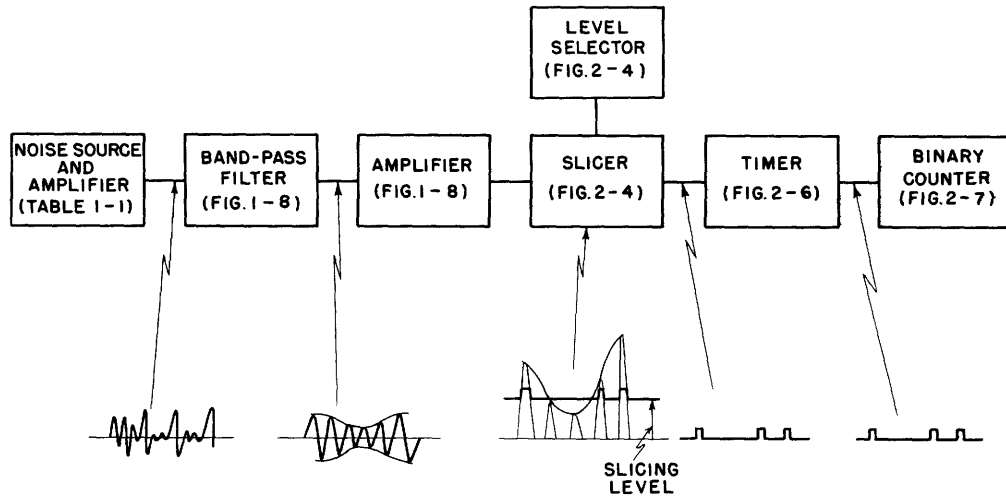

Fig. 2-2 Block diagram for the noise distribution analyzer.

selector. The number of these peaks during an observation time T, controlled by the timer, is registered by the binary counter and called $\#$ counts (X). The envelope distribution function is then simply

$$P(X) = 1 - \frac{\# \text{ counts } (X)}{\# \text{ counts } (0)} \qquad (2\text{-}1)$$

and the distribution density

$$p(X) = \frac{d}{dX} \, P(X) = - \frac{d}{dX} \left(\frac{\# \text{ counts } (X)}{\# \text{ counts } (0)} \right) \qquad (2\text{-}2a)$$

or approximately for finite level steps $\Delta X = X_2 - X_1$

$$p(X) \approx \frac{\# \text{ counts } (X_1) - \# \text{ counts } (X_2)}{X_2 - X_1} \qquad (2\text{-}2b)$$
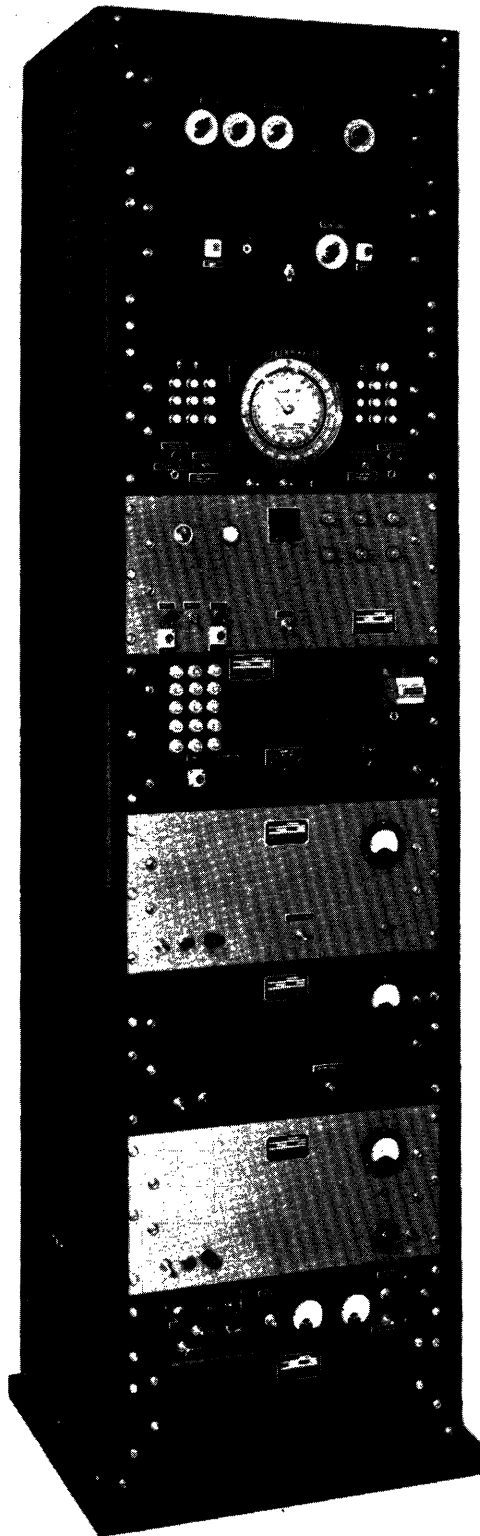
where X_1 and X_2 are adjacent levels.

Figure 2-3 is a photograph of the machine. The chassis in the 8-foot rack are, from top to bottom, the noise source, filter and amplifier (see Section 1.4); slicer; level selector; timer; binary counter; and power supplies. The whole cabinet is shock-mounted.

The different units are described separately below.

2.31   Slicer*

The slicer contains a clipper circuit, 3 slicer circuits and a multivibrator, as shown in Fig. 2-4.

The clipper prevents peaks in excess of the linear region from overloading the slicer circuits. The multivibrator serves to convert the series of variable duration pulses into identical pulses, insuring positive firing of the counter.

2.32   Level selector

The levels should be stable and discrete in order to avoid inaccuracy of resetting to specific points on a continuous scale. Furthermore, it is convenient to have equal voltage steps between successive levels. After having tried different schemes, it was found preferable to use dry element cells.

Thus, the level selector consists of 28 cells in cascade, each of 1.57 volts, with voltage dividers of precision resistors for steps equal to 1/2 (or 1/3) cell voltage. The relationship between steps measured in volts and in number of battery cells is plotted in Fig. 2-5.

Fig. 2-3
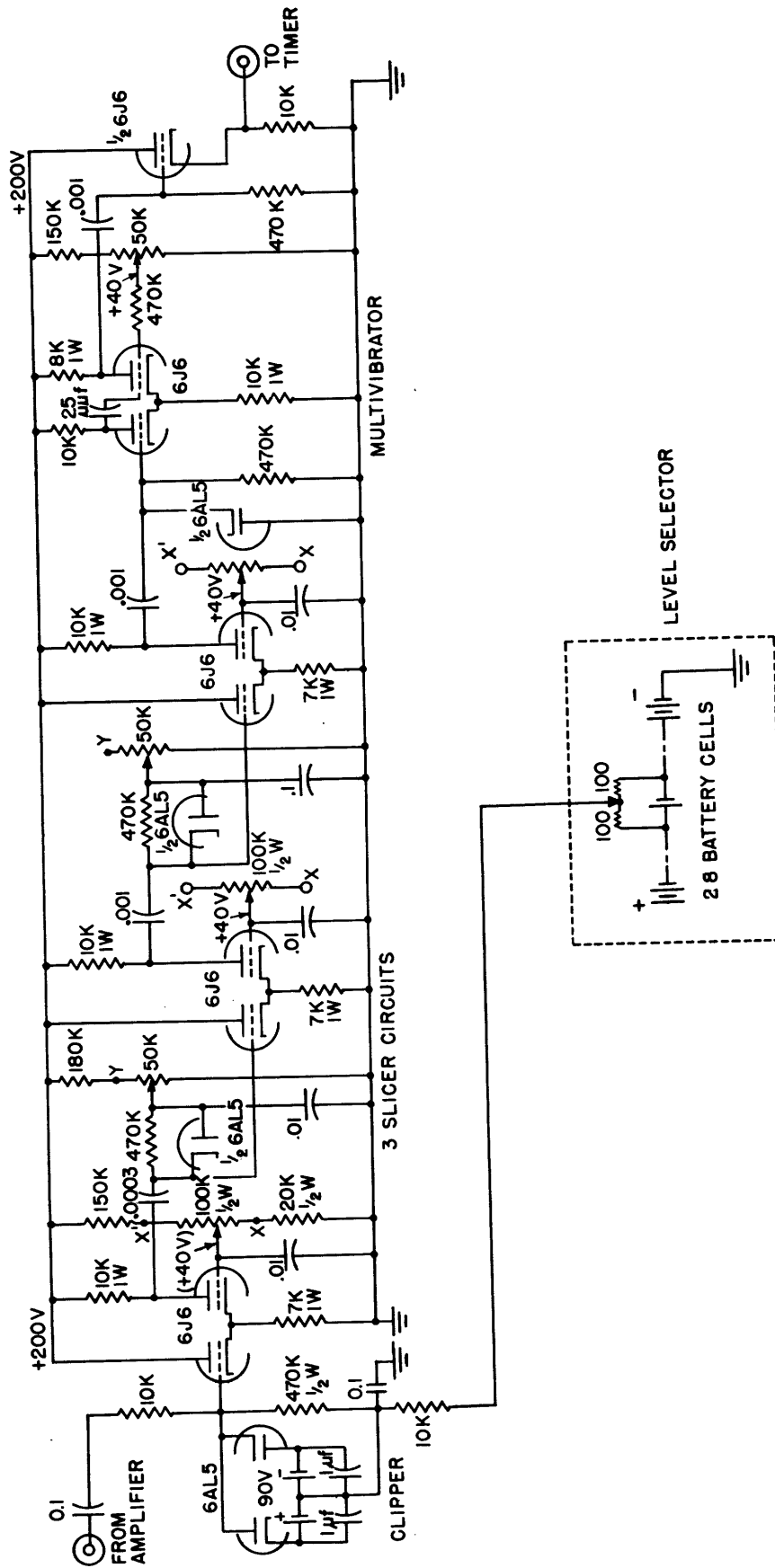Noise distribution analyzer.
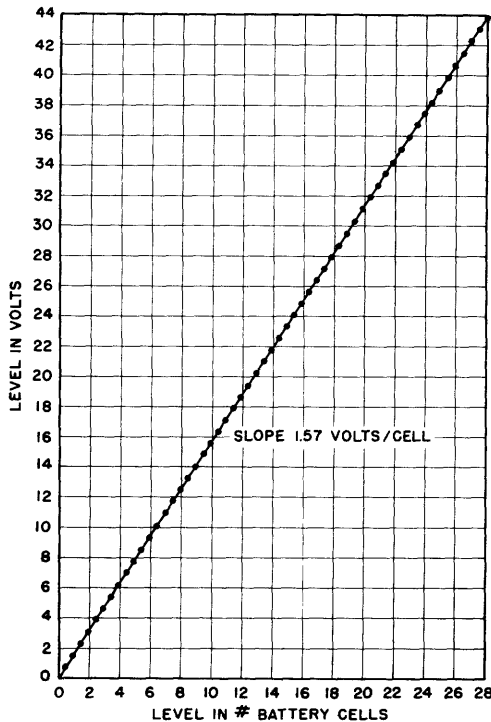
Fig. 2-4 Circuit diagram for slicer.

Fig. 2-5 *Level selector voltage as a function of number of battery cells.*

2.33 Timer

The timer permits connection between slicer and counter by relay contacts for accurate time observation intervals of T = 1,3,7,15 and 31 (i.e. $2^n - 1$) minutes. The latched relay is energized by pulses from cascaded flip-flop frequency dividers timed by a microswitch on a synchronous motor.
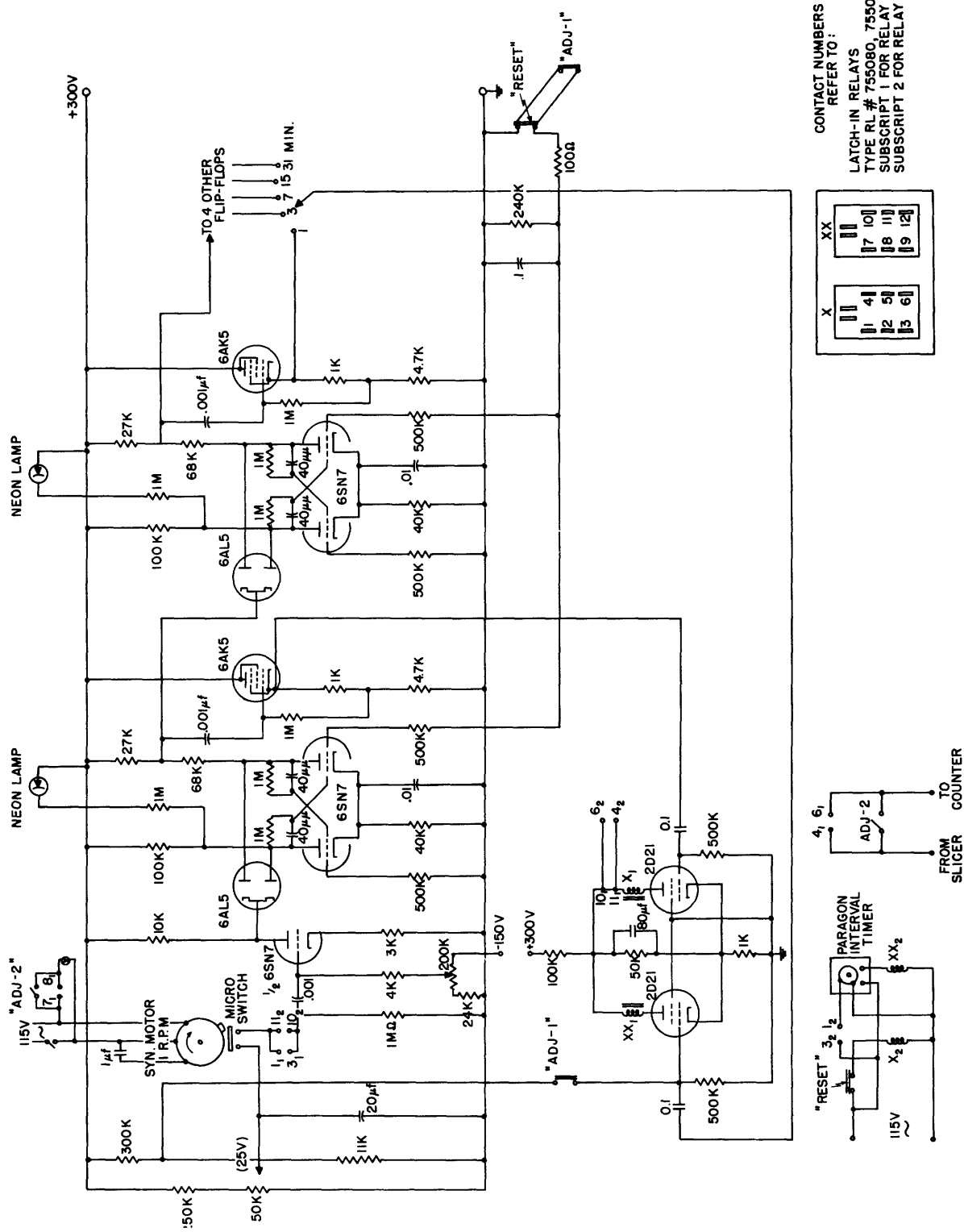
The circuit diagram is given in Fig. 2-6.

2.34 Binary counter

The counter contains 15 flip-flop circuits in cascade and an electrical impulse counter, which can give 1 count for respectively 8, 8^2, 8^3, 8^4 and 8^5 pulses at the input; the intermediate numbers are read from neon lamps.

The circuit diagram is shown in Fig. 2-7.

2.35 Operation

The technique of taking data is quite simple. After selecting the proper noise rms value, observation time, counting rate and slicing level, the machine operates and stops counting automatically. The counter registrations may be recorded at any later time before proceeding to the next level. The factors determining the choice of settings will be discussed in Section 2.5.
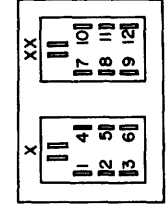
Fig. 2-6 Circuit diagram for timer.
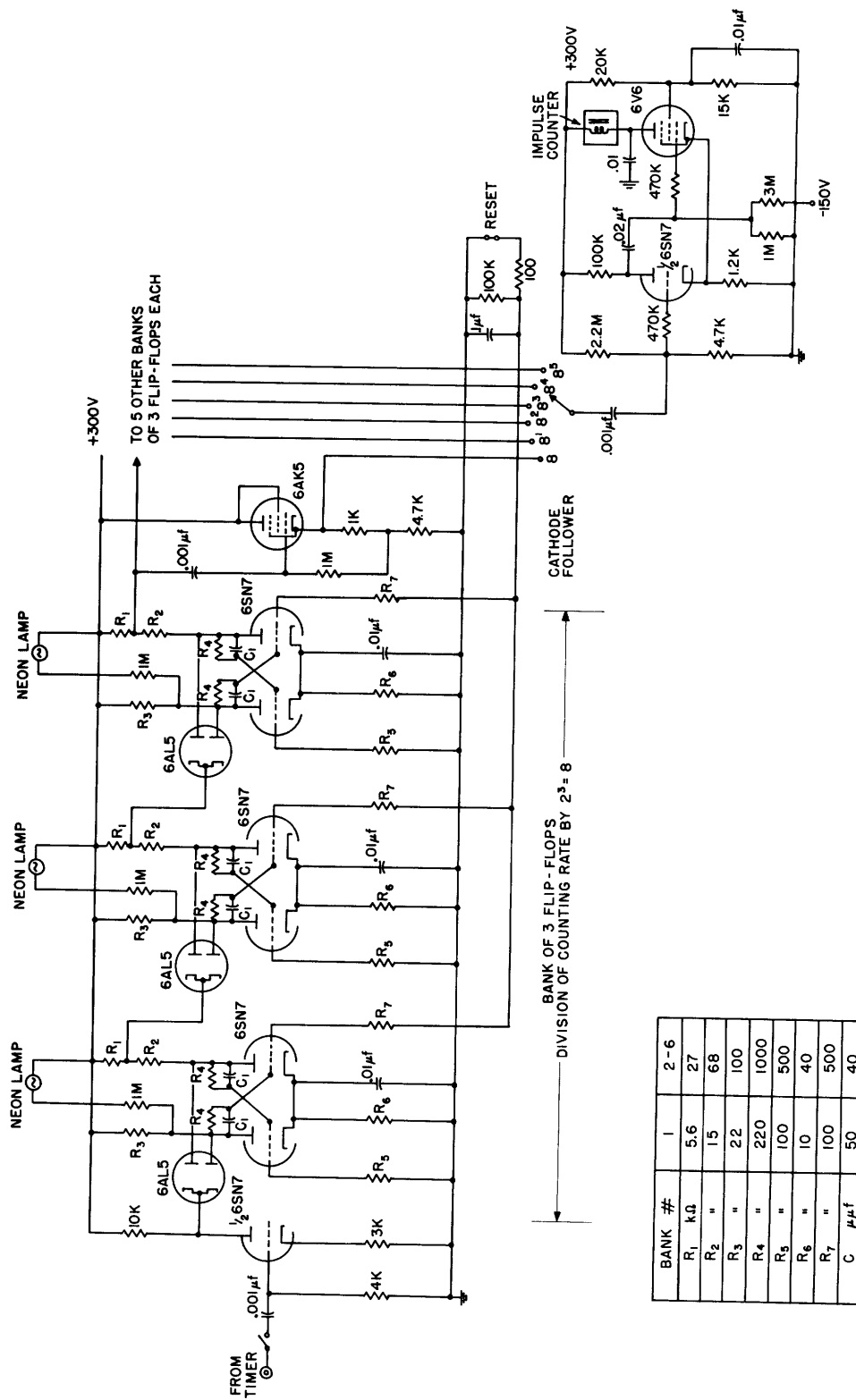
Fig. 2-7 Circuit diagram for binary counter.

BANK #		1	2-6
R_1	kΩ	5.6	27
R_2	"	15	68
R_3	"	22	100
R_4	"	220	1000
R_5	"	100	500
R_6	"	10	40
R_7	"	100	500
C	μf	50	40

-23-

2.4 Experimental Difficulties

2.41 Temperature stability

It will usually take 3 to 4 hours to run a distribution curve, during which time the noise source as well as the rest of the machine must remain in temperature equilibrium in order to give reproducible results. Since the total amplification in some cases (shot and thermal noise through high-Q filters) is of the order of 10^6, the requirements are rather severe.

With the arrangements described in Section 1.2 it was possible to hold the rms value of the noise sources constant, except the Si-crystal.
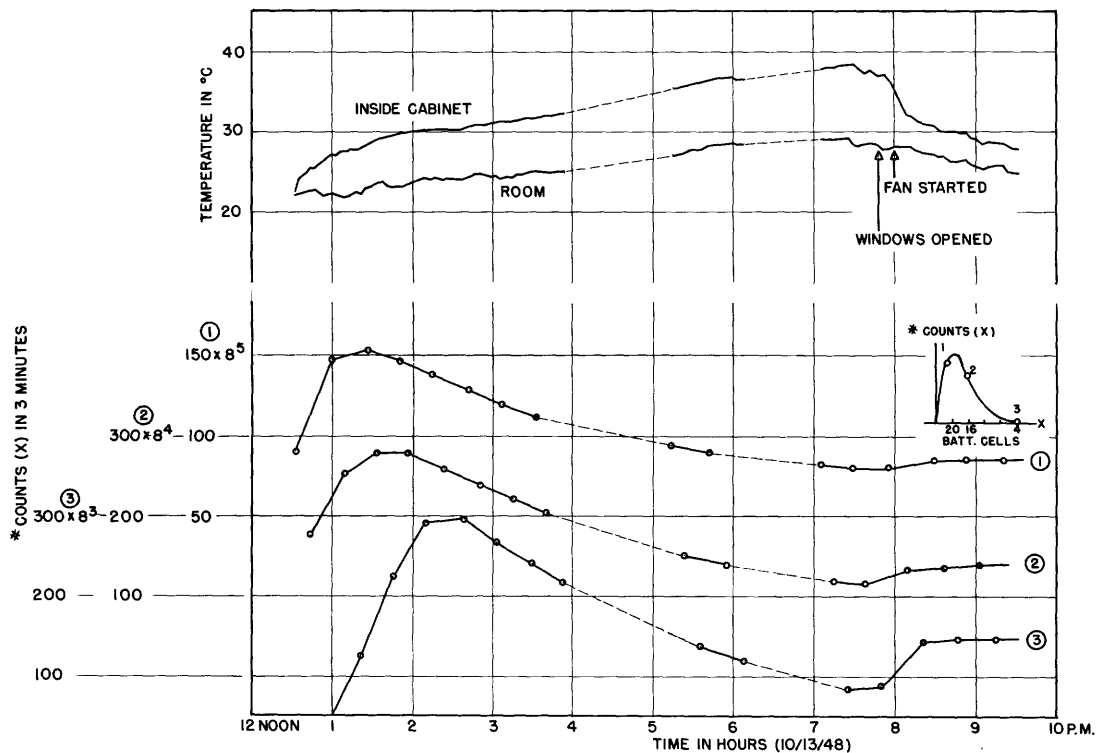
Fig. 2-8 Temperature stability curves for the noise distribution analyzer.

The rest of the machine is mainly affected by the "inner" temperature. Fig. 2-8 shows the dependence of # counts (X) for three different levels, X_1, X_2 and X_3 as a function of time during the warm-up period. It appears that the machine is not stabilized for 8 hours, for this reason it was kept running day and night. Although ambient temperature changes do not seem to influence the # counts (X) appreciably, the room temperature was maintained as constant as possible.

Experience has shown that with adequate precautions it was perfectly possible to get reproducible data for statistical characteristics of random noise from measurements over 3 to 4 hours or even longer. The same results could however be obtained in much shorter time and consequently without the need for such long-time constancy by observing

-24-

all levels at the same time. It should be kept in mind that the advantages of simultaneous observations in many cases of measurements on stationary time series may well justify more complex equipment.

2.42 Rms reading

The meter at the output of the amplifier in Fig. 1-8 was used to read the rms value of the noise. Its indication is important for checking the stability of the noise source and the amplifier, furthermore it determines the normalizing factors for the final results.

A thermocouple precision voltmeter was used, although it was recognized as not being entirely satisfactory for these purposes because of its inherent slowness and frequency dependent behavior.

2.5 Equipment accuracy, adjustments, test

2.51 Accuracy

Each observation was repeated, and the discrepancy held to within 4/8 of one count on the impulse counter. If the difference was greater and could not be traced back to any stability disturbances, the observation time T was increased. Therefore the accuracy was determined experimentally by the reproducibility of observed data. This fundamental and adequate criterion is reflected by the smoothness of the curves obtained.

In order to check for any stability disturbances, the noise display on the scope and the rms meter reading were observed almost continuously, and the number of counts at zero level remeasured at every tenth level.

Increasing the observation time at each level by an increment ΔT, increases the total observation time by 50 (ΔT). Thus, due to the difficulties of long-time constancy, there clearly exists a compromise between the accuracy of measurements at each level and the overall accuracy.

2.52 Adjustments

The observation line T was selected in accordance with the rules derived in Section 2.51.

The rms value was adjusted so that the highest peaks to be measured did not exceed 40 volts, which is the upper limit of the linear range of the slicer.

2.53 Test

The distribution function for a sinusoid is known to be

$$P(X) = \frac{1}{\pi} \cos^{-1} \frac{X}{a}$$

and the distribution density

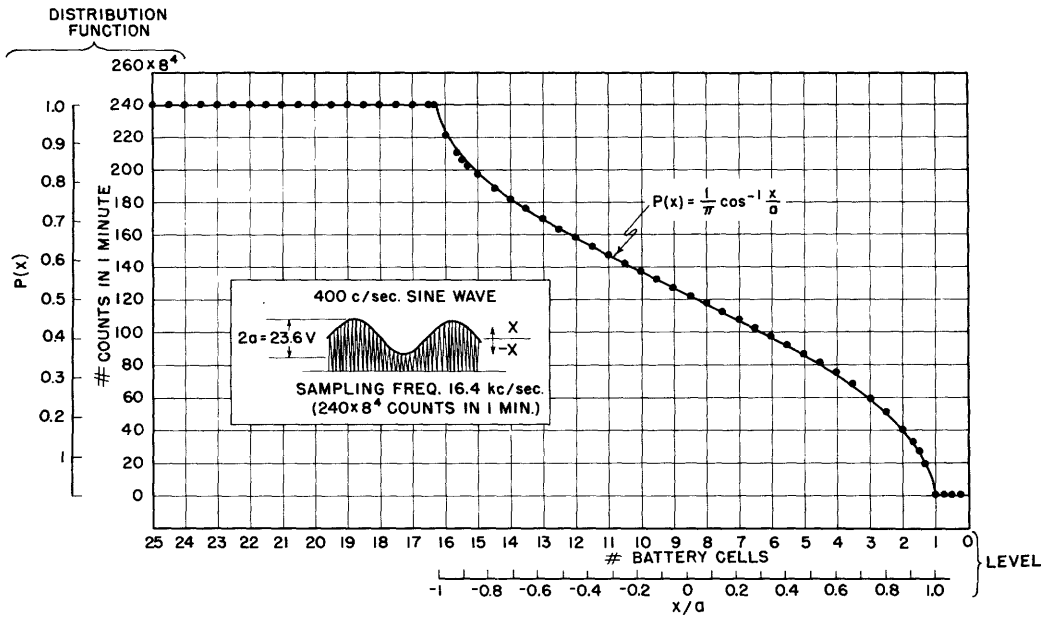$$p(X) = \frac{1}{\pi \sqrt{a^2 - X^2}}$$

Fig. 2-9 Experimental points and theoretical curve for the distribution function of the sinusoidal envelope of an AM wave.
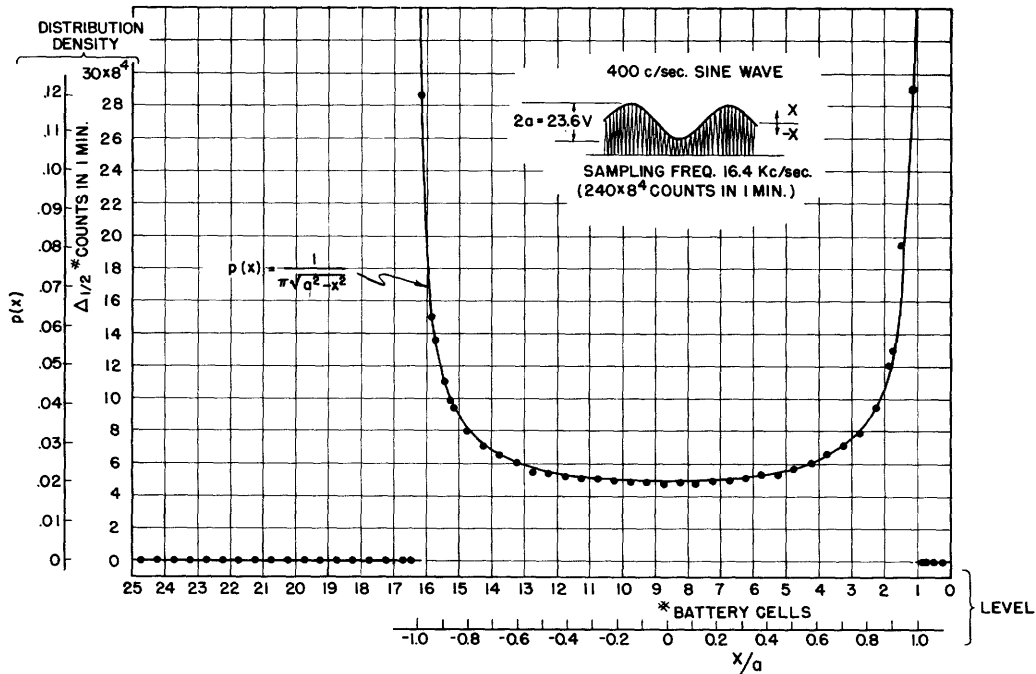

Fig. 2-10 Experimental points and theoretical curve for the distribution density of the sinusoidal envelope of an AM wave.

where

$$X = \text{level}$$
$$a = \text{amplitude} \quad .$$

A convenient and adequate test adopted for the noise distribution analyzer was to measure the envelope distribution of an AM wave modulated by a sinusoid. This time function could be measured by the same method as filtered noise, i.e., sampling of the envelope by means of the instantaneous voltage.

The AM wave was obtained from a G.R. signal generator, type 605B. The carrier was set at 16.4 kc, the modulating frequency at 400 c, and the degree of modulation at 50 percent. The rms value was adjusted so that the maximum peaks were near to 40 volts. The distortion of the envelope was measured to be 1.2 percent second harmonic and 0.6 percent third harmonic.

The experimental points for the distribution function and density respectively are plotted in Figs. 2-9 and 2-10 together with the theoretical curves. The discrepancy is within the limits of expected accuracy.

2.6 Results, Conclusions

2.61 Results

The data are obtained as the number of counts at different levels X, increasing in discrete steps ΔX equal to 1, 1/2 or 1/3 battery cell. The distribution function and density are then determined by Eqs. (2-1) and (2-2b) as functions of the level expressed in number of battery cells.

It is desirable for comparison to normalize the curves with respect to the rms value of the noise $\mathcal{V}$. According to Eqs. (1-4) and (1-5) this is simply accomplished by dividing the abscissas by $\mathcal{V}$ (expressed in number of battery cells), and multiplying the ordinates for the density by $\mathcal{V}/\Delta X$.

The final results for noise from the six sources from various filter combinations are presented in Table 2-1. Both the distribution function and density are shown, since the latter gives the best account at low levels.

For the Si-crystal only the distribution function is shown, since this noise source was unstable with respect to the rms value. However, during intervals of rms constancy, the points for the density fell on corresponding parts of the theoretical Rayleigh curves.

Measurements were in general stopped at levels equal to 4 to 5 times the rms value. Much higher peaks exist, however, as will be seen from Fig. 2-11 for noise from gas tube 884 with filter No. 2, 9.9. Observations were in this case carried on to X = 6.3 times the rms value, where 8 peaks were counted during 5 hours. Although this number is too small for accurate determination of the distribution, it should be noticed that the point is "in line" with the theoretical curve.
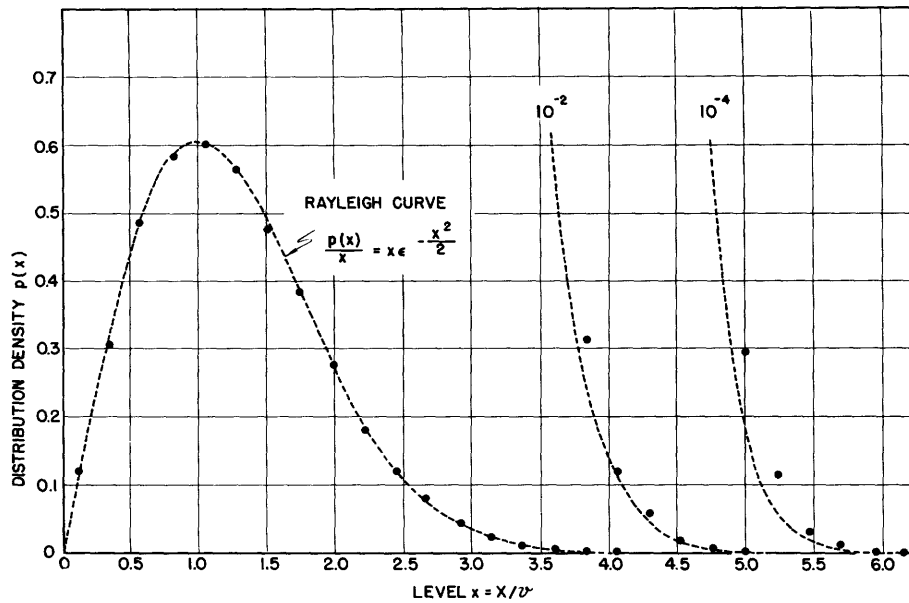
Fig. 2-11 Experimental points and theoretical curve for the
envelope distribution density of noise from gas
tube 884.

2.62 Conclusions

It will be seen from Table 2-1 that the experimental points for the noise envelope distributions are in close agreement with the theoretical Rayleigh curves for all noise sources. From this it may be concluded that the distribution density of the instantaneous noise voltage is Gaussian. The distributions are independent of the Q of the single-tuned circuit through which the noise is passed, at least when Q is varied within the range (108-9.9). The experimental results were reproducible from hour to hour and day to day.

The highest noise peaks observed exceeded 6.3 times the rms value of the noise, but this is certainly not the limit.

TABLE 2-1: NORMALIZED DISTRIBUTIONS

NOISE SOURCE AND TYPE FILTER NUMBER R.M.S. VALUE OBSERVATION DATE	ENVELOPE DISTRIBUTION FUNCTION	ENVELOPE DISTRIBUTION DENSITY
GAS TUBE 884 ○ FILTER NO. 2, 26.6 R.M.S. 7.5 V OBS. 3/3/49 ● FILTER NO. 2, 9.9 R.M.S. 7.5 V OBS. 3/4/49		
BALLANTINE AMPLIFIERS, MODEL 300 SHOT AND THERMAL NOISE ○ FILTER NO. 1, 26.6 R.M.S. 8.05 V OBS. 2/20/49 ● FILTER NO. 2, 26.6 R.M.S. 8.0 V OBS. 3/1/49		
G.R. AMPLIFIER, TYPE 1231-B THERMAL NOISE ○ FILTER NO. 4 x 2, 108 R.M.S. 6.45 V OBS. 4/7/49 ● FILTER NO. 4 x 2, 26.6 R.M.S. 7.5 V OBS. 2/23/49		

-29-

EIMAC 15 E
SPACE-CHARGE LIMITED
SHOT NOISE

○ { FILTER NO. 2,108
R.M.S. 6.9 V
OBS. 4/3/49

● { FILTER NO. 2,26.6
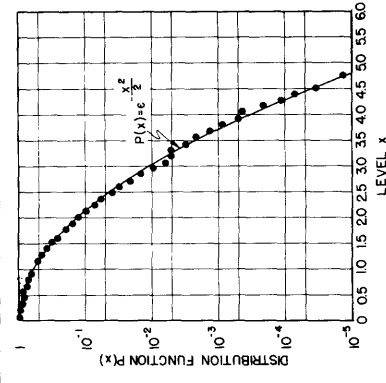R.M.S. 6.9 V
OBS. 4/3/49
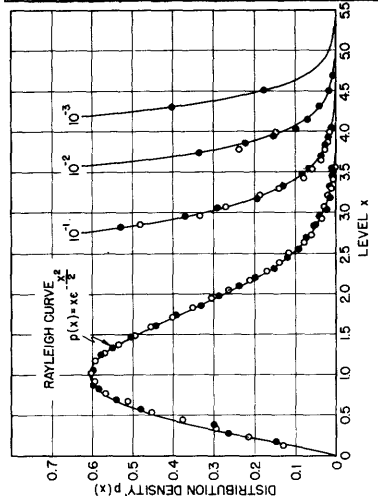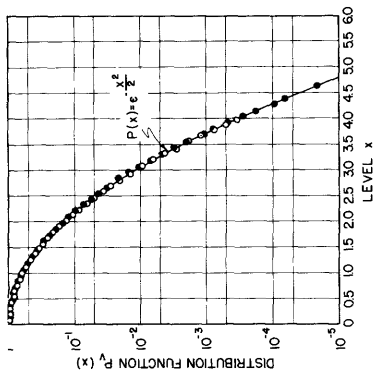
EIMAC 15 E
TEMPERATURE LIMITED
SHOT NOISE

○ { FILTER NO. 2,108
R.M.S. 6.4 V
OBS. 4/2/49
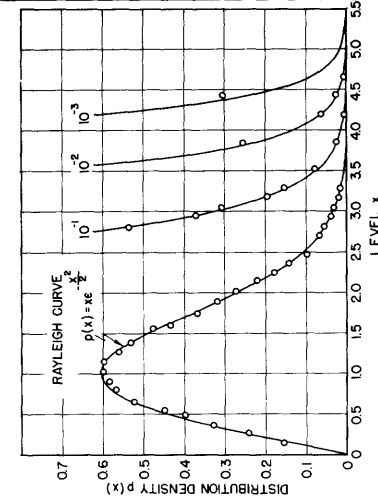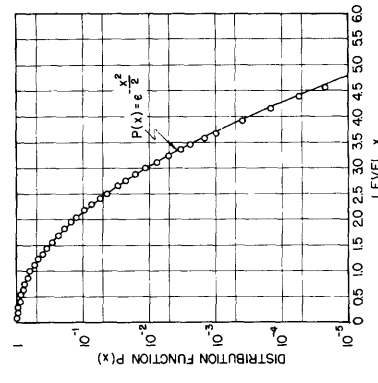
SI-CRYSTAL

● { FILTER NO. 4 x 3 x 2, 4
R.M.S. 6.1- 6.4 V
OBS. 4/4/49

DISTRIBUTION FUNCTION P$_v$(x)

$P(x) = e^{-\frac{x^2}{2}}$

LEVEL x

DISTRIBUTION DENSITY p(x)

RAYLEIGH CURVE

$p(x) = xe^{-\frac{x^2}{2}}$

LEVEL x

PART 3. ZERO-CROSSINGS, AUTOCORRELATION, POWER SPECTRA

This part contains statistical data dependent on the Q (or damping) of the filters through which the noise is passed.

3.1 Zero-Crossings

3.11 Method and results

The average zero-crossing frequency f_z for the narrow-band noise was measured according to its definition in Section 1.3 as the number of peaks exceeding zero level.

The results are presented in Table 3-1. In all cases f_z appears to be proportional to the bandwidth $W = f_o/Q$, but there is a considerable difference with respect to both magnitudes and slopes.

All measurements were repeated after several hours or days, and were reproducible within ± 0.2 percent.

3.12 Discussion

The results can be explained by considering the associated transfer characteristics in Table 1-2. They may be classified in three different classes A, B and C, depending upon their cut-off frequency relative to the center frequency f_o of the single-tuned circuit as sketched in Fig. 3-1. It may be deduced that

filter No. 1   belongs to Class A

filter No. 2   belongs to Class B

filter No. (6 x) 4 x 3 x 2   belongs to Class C

filter No. 5 x 2   belongs to Class BC
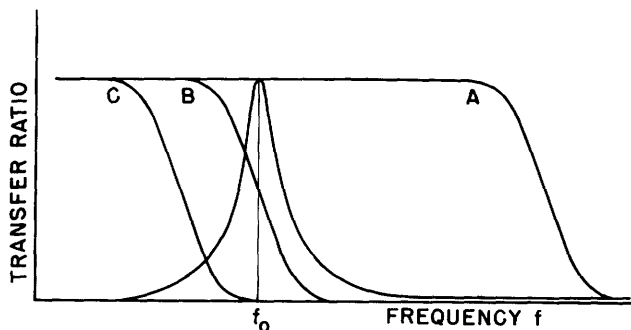
filter No. 4 x 3 x 2   belongs to Class B

Fig. 3-1 Classification of transfer characteristics.

In addition it should be noted that the "gyration frequency" f_z corresponding to the single-tuned circuit alone always is greater than its resonance frequency f_o due to the inherent unsymmetrical shape, see Fig. 3-2.

It is apparent from Fig. 3-1 that for Class A the resultant f_z will be greater than f_o, and for Class B and C less than f_o. Furthermore, it is evident that f_z must increase with the bandwidth $W = f_o/Q$ for Class A and B, but decrease with W for Class C. On the basis of these conclusions, typical curves for f_z as a function of W are plotted in Fig. 3-3. Comparison with the results in Table 3-1 shows qualitative agreement.

TABLE 3-1: AVERAGE ZERO-CROSSING FREQUENCY FOR NOISE VOLTAGE

$$W = \text{BANDWIDTH} = f_0/Q$$

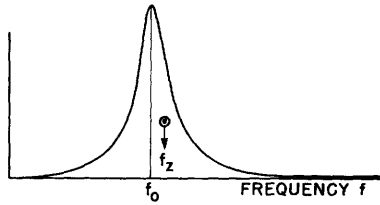| NOISE { SOURCE TYPE	FILTER CODE NUMBER	EXPERIMENTAL CURVES
GAS TUBE 884	2, $Q_{VAR.}$	f_z IN kc vs. W IN c
BALLANTINE AMPLIFIERS MODEL 300 SHOT AND THERMAL NOISE	○ 1, $Q_{VAR.}$ ● 2, $Q_{VAR.}$	f_z IN kc vs. W IN c
G.R. AMPLIFIER TYPE 1231-B THERMAL NOISE	6 4 x 3 x 2, $Q_{VAR.}$	f_z IN kc vs. W IN c
EIMAC 15E SPACE-CHARGE LIMITED SHOT NOISE	5 x 2, $Q_{VAR.}$	f_z IN kc vs. W IN c
EIMAC 15E TEMPERATURE LIMITED SHOT NOISE	5 x 2, $Q_{VAR.}$	f_z IN kc vs. W IN c
SI – CRYSTAL	4 x 3 x 2, $Q_{VAR.}$	f_z IN kc vs. W IN c

-32-

Fig. 3-2

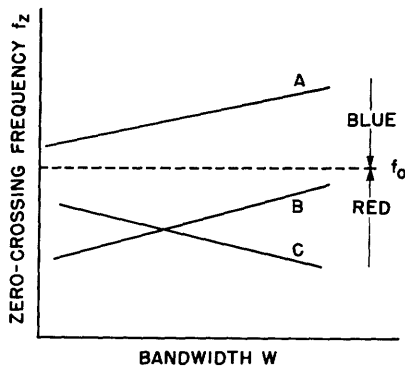Gyration frequency f_z resonance frequency f_o for single-tuned circuit.

Fig. 3-3

Zero-crossing frequency as a function of bandwidth, for transfer characteristics A, B and C.
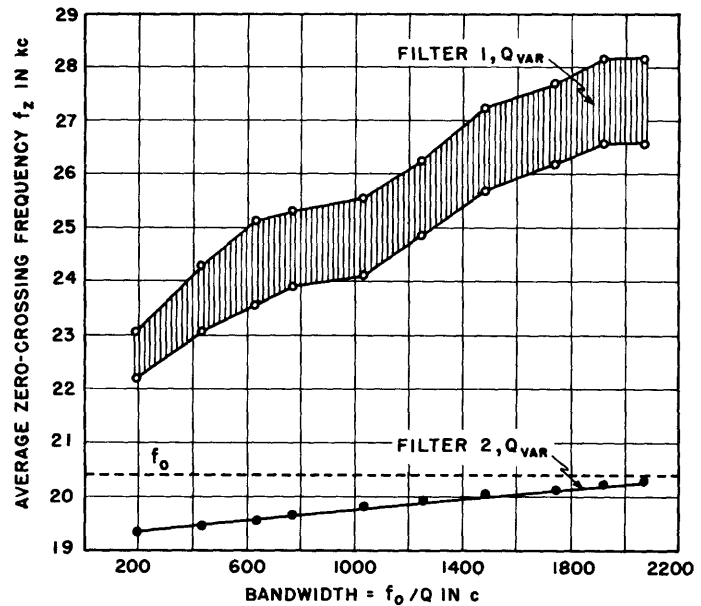

Fig. 3-4

Zero-crossing frequency as a function of bandwidth for gas tube 884 with $(2,Q_{var})$ and without $(1,Q_{var})$ Butterworth low-pass filter.

It is suggestive and also convenient to term the noise at "red" and "blue" respectively when the average zero-crossing frequency is less or greater than the resonance or center frequency of the band-pass filter.

The discrepancy between the curves in Table 3-1 for the gas tube and Ballantine noise in the case of filter No. 2, Q_{var} is due to different initial power spectra for these two sources.

The results in Fig. 3-4 for gas tube noise clearly demonstrates the distinct and unstable high frequency content in the power spectrum of this noise source. The curve for filter No. 2, Q_{var} is fixed, whereas for filter No. 1, Q_{var} the experimental points fell within the shaded region and were otherwise unreproducible.

3.2   Autocorrelation Functions and Power Spectra

Due to the unique relationship of Eqs. (1-9) and (1-10), neither the autocorrelation function nor the power spectrum actually tells more than the other. The choice between working in the time or frequency domain is only a matter of practical considerations. Thus, present day electronic technique is in favor of the time domain, since it appears in general more feasible and less expensive to build adequate pulse timing circuits than

filters. As far as the final representation of results is concerned, a combination seems more profitable since the power spectrum emphasizes the long time shift and low frequency characteristics of the time function, whereas the autocorrelation function gives the best account of the high frequency and short time shift characteristics.

It was pointed out in Section 1.4 that the "correlation method" for obtaining the power spectrum has proved itself extremely useful in theoretical investigations. Since an electronic correlator and an electronic differential analyzer capable of performing Fourier transformations were available, an analogous experimental procedure suggested itself.

3.21 Methods and results*

The filtered random noise at the output of the amplifier, shown in Fig. 1-8, was fed into the electronic correlator. Its operation is described in detail elsewhere (9), it is therefore sufficient to summarize here that the noise is sampled periodically at the rate f_s in pairs τ_k sec apart, the sampled values a_n and b_n are then multiplied, and the products integrated and averaged over the observation time T, according to the formulae

$$\phi(\tau_k) \approx \frac{1}{Tf_s} \sum_{n=1}^{Tf_s} a_n b_n$$

whereafter the machine automatically switches to τ_{k+1}, and so on. The calibrations used were T = 2 min., f_s = 500 c, and total range of time shifts Σ_T = 0.45 ms and 0.11 ms respectively. The rms value of the noise at the input was held as constant as possible at 2.7 volts.

Only filtered noise from gas tube 884 and the Si-crystal were investigated, since these noise sources had betrayed peculiar properties. The autocorrelation functions as recorded by the correlator are presented in the left-hand half of Table 3-2.

These curves are plotted in linear coordinates, and reproduced photographically as masks for the function generator in the differential analyzer (10). Pictures of the corresponding traces on the scope are shown in the right-hand half of Table 3-2 together with the power spectra obtained. The frequency scale is linear.

All correlation curves were reproducible within ±4 percent of the maximum value. The system error introduced by the differential analyzer is best estimated by the discrepancy between the traces of the power spectrum and zero line at the higher frequencies.

3.22 Discussion

The autocorrelation functions for noise through single-tuned circuits as shown to the left in the 3rd, 4th and 6th row of Table 3-2 are damped cosine waves with damping constant depending on the Q. This is in agreement with the conclusions in Section 1.14.

TABLE 3-2

AUTOCORRELATION FUNCTIONS $\phi_{11}(\tau)$ REGISTERED BY CORRELATOR		AUTOCORRELATION FUNCTIONS $\phi_{11}(\tau)$ REGISTERED BY FUNCTION GENERATOR	POWER SPECTRA $\phi_{11}(f)$ REGISTERED BY DIFFERENTIAL ANALYZER	NOISE TYPE R.M.S. VALUE FILTER CODE NO.
0 0.1 0.2 0.3 0.4 0.45 TIME τ IN ms	0 002 004 006 008 010 011 TIME τ IN ms	0 002 004 006 008 010 011 TIME τ IN ms	0 10 20 30 40 50 60 FREQUENCY f IN kc	
				884 GAS TUBE NOISE R.M.S.=2.7 V FILTER: 1, —
				884 GAS TUBE NOIS R.M.S.=2.7 V FILTER: 2, —
				884 GAS TUBE NOISE R.M.S.=2.7 V FILTER: 1, 9.9
				884 GAS TUBE NOISE R.M.S.=2.6 V FILTER: 1, 108.4
				S1-CRYSTAL NOISE R.M.S.=2.7-3.0V FILTER: 4x1
				S1-CRYSTAL NOISE R.M.S.=2.6-2.8V FILTER: 4x1, 26.6

The autocorrelation functions and power spectra for broadband noise from gas tube 884 in the 1st and 2nd row show interesting features. Filter No. 1 passes the distinct high frequency mode (probably plasma oscillations) the effect of which already has been pointed out in connection with the photographs in Section 1.6 and the zero-crossing curve in Fig. 3-4. With filter No. 2 this perturbation is removed.

From the 5th row in Table 3-2 it will be seen that the noise from the Si-crystal is concentrated in the lower frequency region.

Wiener (11) has suggested a method of determining the system function $H(\omega)$ from the input and output power spectra, $\Phi_i(\omega)$ and $\Phi_o(\omega)$, according to the formulae

$$|H(\omega)|^2 = \frac{\Phi_o(\omega)}{\Phi_i(\omega)} \quad .$$

The experimental "correlation method" for obtaining the power spectra, as demonstrated above, may be useful for this particular application, since it in many cases is more flexible than direct frequency measurements.

The experimental results obtained from photographs and measurements of envelope distribution, zero-crossings, autocorrelation and power spectra are in agreement with the theory. Mutual influence of incoherent signal and noise has not been considered, since superposition applies in linear systems.

There appear to be no insurmountable difficulties in extending similar noise measurements'to nonlinear systems, whereas the theory becomes extremely complicated. Consequently, the experimental approach promises to be the more appropriate in future investigations.

References

(1) S. O. Rice: Mathematical analysis of random noise, B.S.T.J., July 1944, pp. 282-332; January 1945, pp. 46-156.

(2) Y. W. Lee, C. A. Stutt: Statistical prediction of noise, Technical Report No. 129, Research Laboratory of Electronics, M.I.T., 1949.

(3) J. D. Cobine, C. J. Gallagher; Noise and oscillations in hot cathode arcs, J. Frank. Inst., January 1947, pp. 41-54.

(4) J. D. Cobine, C. J. Gallagher: Effect of magnetic field on noise and oscillations in hot cathode arcs, J. Appl. Phys., January 1947, pp. 110-116.

(5) Quarterly Progress Report, Research Laboratory of Electronics, M.I.T., January 15, 1948, p. 51.

(6) Quarterly Progress Report, Research Laboratory of Electronics, M.I.T. April 15, 1948, pp. 49-52.

(7) E. J. Pumper: A method for experimental investigation of the number of large deviations in electric fluctuations, C. R. de l'Acad. des Sciences USSR, LlII, 1 1946, pp. 25-27.

(8) R. Fürth, D. K. C. MacDonald: Statistical analysis of spontaneous electrical fluctuations, Proc. of the Phys. Soc., LIX, 1947, pp. 388-403.

(9) Quarterly Progress Report, Research Laboratory of Electronics, M.I.T., July 15, 1948, pp. 60-64.

(10) A. B. Macnee: An electronic differential analyzer, Technical Report No. 90, Research Laboratory of Electronics, M.I.T., 1948.

(11) N. Wiener: Generalized harmonic analysis, Acta Math., 55, 1930, pp. 117-258.